Científica

vol. 30, no. 2, July-December 2026, pp. 01-16
ISSN 2594-2921, Instituto Politécnico Nacional, MÉXICO
e300211 | DOI: 10.46842/ipn.cien.v30n2a11

ARTICLE

Task-Specific β_1 and β_2 Dual-Slope Spectral Features of fNIRS Signals for Parkinson's Disease Classification

Características espectrales de doble pendiente β_1 y β_2 específicas de cada tarea en las señales fNIRS para la clasificación de la enfermedad de Parkinson

Jesús Fausto **Córdova Manzo** [1]
Daniel **Acosta Mares** [2]
Gabriela **Flores Mondragón** [3]
Cinthya Lourdes **Toledo Peral** [4]
Gabriel **Vega Martínez** [5]
Arturo **Vera Hernández** [6]
Edgar **Guevara** [7]

Centro de Investigación y de Estudios Avanzados,
Electrical Engineering Department, Ciudad de México, MÉXICO
[1] ORCID: 0000-0001-6284-6990 / jesus.cordovam@cinvestav.mx
[6] ORCID: 0000-0001-6258-154X / arvera@cinvestav.mx

Universidad Autónoma de San Luis Potosí,
Faculty of Engineering/Faculty of Sciences, San Luis Potosí, MÉXICO
[2] ORCID: 0009-0004-2981-0995 / daniel.acostam@uaslp.mx
Faculty of Sciences, San Luis Potosí, MÉXICO
[7] ORCID: 0000-0002-2313-2810 / edgar.guevara@uaslp.mx

Instituto Nacional de Rehabilitación Luis Guillermo Ibarra Ibarra,
Basic Neurosciences Service, Ciudad de México, MÉXICO
[3] ORCID: 0000-0002-2275-495X / gaflores@inr.gob.mx
Division for Research in Medical Engineering, Ciudad de México, MÉXICO
[4] ORCID: 0000-0003-0522-1155 / phd.toledo@outlook.com
[5] ORCID: 0000-0002-3984-7124 / gvega@inr.gob.mx

https://científica.site

Recibido 02/11/2026, aceptado 25/11/2026, publicado 30-11-2026.

 Creative Commons License: Attribution-NonCommercial-ShareAlike 4.0 International CC BY-NC-SA 4.0

Abstract

Parkinson's disease (PD) is associated with altered motor-network function, motivating the search for objective neurophysiological features capable of complementing clinical assessment. This exploratory secondary study investigated whether the frequency-domain morphology of functional near-infrared spectroscopy (fNIRS) signals could be represented by two task-specific spectral slopes, β_1 and β_2, and whether their multivariate combination could discriminate participants with PD from healthy controls. The source cohort comprised 20 participants with PD and 20 age- and sex-matched controls evaluated during resting state, finger tapping, and walking. Final continuous hemoglobin concentration signals obtained after channel-quality pruning, optical-density conversion, motion-artifact identification and correction, temporal filtering, and conversion to hemoglobin concentration using the modified Beer–Lambert law were analyzed without additional temporal band-pass filtering. Timestamp-based quality control identified recordings acquired at 25, 50, and 75 Hz; recordings above 25 Hz were harmonized to 25 Hz by polyphase resampling. Common analysis durations of 265 s for resting state, 590 s for finger tapping, and 118 s for walking yielded 36 participants with complete three-task data (17 controls and 19 PD). Power spectral density was estimated using Welch's method, and a continuous two-segment regression was fitted in log10[P(f)] versus log10(f) space. β_1 and β_2 were extracted for HbO, HbR, and HbT across the three tasks, yielding 18 participant-level features. Four exploratory spectral configurations were evaluated using fixed or automatically optimized crossover frequencies and upper bounds of 10 or 12.5 Hz. Classification used feature standardization, principal component analysis retaining 95% of the variance, L2-regularized logistic regression, leave-one-subject-out cross-validation, and 500 label permutations. Fixed-12.5 achieved the highest threshold-dependent performance, with 86.1% accuracy, 86.2% balanced accuracy, 84.2% sensitivity, 88.2% specificity, MCC = 0.723, and ROC-AUC = 0.820. Auto-10 achieved the highest ROC-AUC (0.827) and the best spectral-model fit, with global median NRMSE = 0.0346, $R_1^2 = 0.875$, $R_2^2 = 0.984$, and total $R^2 = 0.989$. All four configurations performed significantly above their corresponding permutation null distributions. These findings indicate that compact task-dependent dual-slope spectral descriptors of preprocessed fNIRS concentration signals contain multivariate information associated with PD status. Because the analyzed signals had already undergone these preprocessing operations, β1 and β2 are interpreted primarily as empirical descriptors of spectral morphology rather than direct estimates of intrinsic physiological power-law scaling. Independent validation using a locked analytical pipeline and an external cohort is required before diagnostic interpretation.

Index terms: Parkinson's disease, functional near-infrared spectroscopy, power spectral density, spectral slope, machine learning, motor cortex.

Resumen

La enfermedad de Parkinson (EP) se asocia con alteraciones en el funcionamiento de las redes motoras, lo que ha motivado la búsqueda de características neurofisiológicas objetivas capaces de complementar la evaluación clínica. En este estudio secundario exploratorio se investigó si la morfología en el dominio de la frecuencia de las señales de espectroscopia funcional de infrarrojo cercano (fNIRS) podía representarse mediante dos pendientes espectrales específicas de la tarea, β_1 y β_2, y si su combinación multivariada permitía discriminar participantes con EP de controles sanos. La cohorte original estuvo constituida por 20 participantes con EP y 20 controles pareados por edad y sexo, evaluados durante reposo, finger tapping y marcha. Se analizaron las señales continuas finales de concentración de hemoglobina obtenidas después de la depuración de canales por calidad, conversión a densidad óptica, identificación y corrección de artefactos de movimiento, filtrado temporal y conversión a concentración de hemoglobina mediante la ley de Beer-Lambert modificada, sin aplicar un filtrado temporal adicional de paso de banda. El control de calidad basado en las marcas temporales identificó registros adquiridos a 25, 50 y 75 Hz; aquellos adquiridos por encima de 25 Hz se armonizaron a 25 Hz mediante remuestreo polifásico. Se establecieron duraciones comunes de 265 s para reposo, 590 s para finger tapping y 118 s para marcha, obteniéndose 36 participantes con información completa en las tres tareas (17 controles y 19 con EP). La densidad espectral de potencia se estimó mediante el método de Welch y se ajustó una regresión continua de dos segmentos en el espacio log10[P(f)] frente a log10(f). Se extrajeron β_1 y β_2 para HbO, HbR y HbT en las tres tareas, generando 18 características por participante. Se evaluaron cuatro configuraciones espectrales exploratorias con frecuencias de cruce fijas u optimizadas automáticamente y límites superiores de 10 o 12.5 Hz. La clasificación utilizó estandarización de características, análisis de componentes principales con retención del 95% de la varianza, regresión logística con regularización L2, validación leave-one-subject-out y 500 permutaciones de las etiquetas. Fixed-12.5 presentó el mayor rendimiento dependiente del umbral, con 86.1% de exactitud, 86.2% de exactitud balanceada, 84.2% de sensibilidad, 88.2% de especificidad, MCC = 0.723 y ROC-AUC = 0.820. Auto-10 presentó el ROC-AUC más alto (0.827) y el mejor ajuste espectral, con NRMSE mediano global = 0.0346, $R_1^2 = 0.875$, $R_2^2 = 0.984$ y R^2 total = 0.989. Las cuatro configuraciones mostraron un desempeño significativamente superior a sus correspondientes distribuciones nulas obtenidas por permutación. Estos hallazgos indican que los descriptores espectrales compactos de doble pendiente dependientes de la tarea, extraídos de señales de concentración fNIRS preprocesadas, contienen información multivariada asociada con la EP. Debido a que las señales analizadas ya habían sido previamente procesadas, β_1 y β_2 se interpretan principalmente como descriptores empíricos de la morfología espectral y no como estimaciones directas de una ley de potencia fisiológica intrínseca. Se requiere validación independiente mediante un flujo analítico previamente fijado y una cohorte externa antes de considerar una interpretación diagnóstica.

Palabras clave: enfermedad de Parkinson, espectroscopia funcional de infrarrojo cercano, densidad espectral de potencia, pendiente espectral, aprendizaje automático, corteza motora.

CC BY-NC-SA 4.0

I. INTRODUCTION

Parkinson's disease (PD) is a progressive neurodegenerative disorder whose cardinal motor manifestations include bradykinesia, rigidity, resting tremor, and postural instability. Although degeneration of nigrostriatal dopaminergic pathways constitutes a central component of the disease, PD is increasingly understood as a disorder involving distributed motor and non-motor networks. Diagnosis nevertheless remains fundamentally clinical, motivating continued investigation of neurophysiological measurements capable of quantitatively characterizing disease-associated alterations [1], [2].

Functional near-infrared spectroscopy (fNIRS) is particularly attractive in the study of movement disorders because it provides non-invasive measurements of cortical hemodynamic changes while allowing participants to perform tasks that would be difficult to reproduce under conventional neuroimaging constraints. Changes in oxygenated hemoglobin (HbO), deoxygenated hemoglobin (HbR), and total hemoglobin (HbT) provide complementary descriptions of task- and state-dependent hemodynamic activity [3].

Previous analyses of the cohort examined in the present work demonstrated that PD-related abnormalities are detectable in bilateral motor-cortex fNIRS recordings. Guevara et al. reported delayed hemodynamic responses during fine finger movements together with reduced interhemispheric resting-state connectivity in participants with PD [4]. A subsequent graph-theoretical analysis identified reduced clustering and small-world organization and a bilateral disconnected subnetwork involving motor and somatosensory regions in PD [5].

Machine-learning approaches have also demonstrated that fNIRS contains multivariate information relevant to PD classification. Guevara et al. extracted a large library of temporal and spectral features and used logistic-regression-based feature-selection strategies to classify PD and control participants [6]. These results motivate the search for lower-dimensional representations that preserve useful discriminative information while remaining easier to interpret and reproduce.

Frequency-domain representations describe how signal variance is distributed across temporal scales. fNIRS signals can exhibit fractal or scale-dependent temporal structure [7], and measures of scale invariance have been shown to vary with brain state and task demands [8]. For approximately scale-dependent signals, spectral power can be described by $P(f) \propto f^{-\beta}$, such that β corresponds to the negative slope of the power spectral density in logarithmic coordinates. However, biological and processed physiological signals do not necessarily exhibit one linear log-log relationship across an entire frequency interval. Changes in spectral slope can produce distinct regions separated by a crossover frequency f_c. Exploratory inspection of the present post-Homer3 spectra suggested task-dependent changes in slope, motivating a compact two-segment representation based on β_1 for the lower-frequency region and β_2 for the higher-frequency region.

The aim of this exploratory secondary study was to determine whether task-specific dual-slope spectral features extracted from post-Homer3 fNIRS signals could discriminate participants with PD from healthy controls. We additionally evaluated whether fixed or automatically derived crossover frequencies provided the most consistent representation of spectral morphology and whether classification performance remained robust across alternative spectral parameterizations. Fig. 1 summarizes the complete analytical workflow.

CC BY-NC-SA 4.0

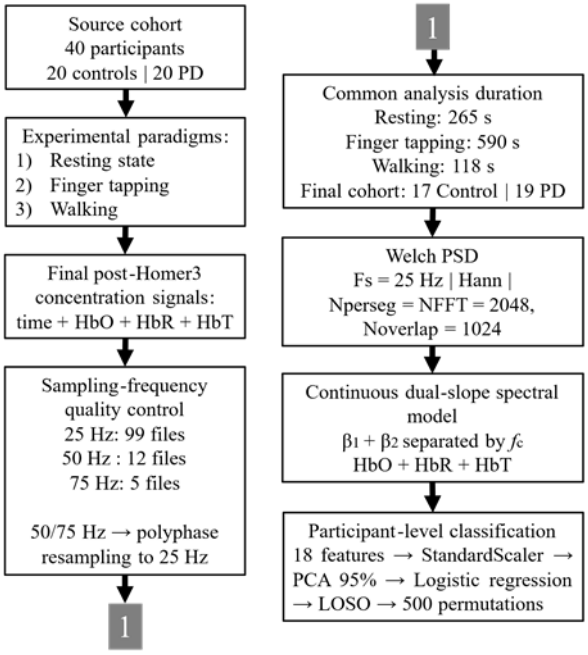

Fig. 1. Overall analytical workflow of the study. Final post-Homer3 concentration signals from resting state, finger tapping, and walking were subjected to sampling-frequency quality control, harmonization to 25 Hz when required, task-specific duration standardization, Welch power spectral density estimation, continuous dual-slope modeling, participant-level β1 and β2 feature extraction, dimensionality reduction by principal component analysis (PCA), logistic-regression classification, leave-one-subject-out (LOSO) validation, and permutation testing.

II. Materials and Methods

A. Study Design and Participants

The present work was a secondary exploratory analysis of previously acquired bilateral motor-cortex fNIRS recordings. The source cohort included 20 participants with PD and 20 age- and sex-matched healthy controls. PD diagnosis followed the United Kingdom Parkinson's Disease Society Brain Bank criteria. Disease severity was assessed using the MDS-UPDRS part III and Hoehn and Yahr scales, and participants with PD were evaluated in the practically defined OFF-medication state, approximately 12 h after the last antiparkinsonian medication dose. Global cognitive function was assessed with the Spanish version of the Montreal Cognitive Assessment (MoCA). All participants were right-handed [4].

The original cohort had mean ages of 69.9 ± 10.1 years in the PD group and 65.6 ± 9.9 years in controls. The proportion of men was 60% and 45%, respectively. Mean education was 9.3 ± 4.1 versus 12.1 ± 5.2 years, and mean MoCA scores were 21.6 ± 3.8 versus 26.2 ± 2.7. Participants with PD had a mean MDS-UPDRS III score of 37.4 ± 18.6, disease duration of 8.2 ± 3.8 years, and mean Hoehn and Yahr stage of 2.9 [4].

The study protocol complied with the Declaration of Helsinki and was approved by the Institutional Review Board under registration 77-21. Written informed consent was obtained from all participants [4].

CC BY-NC-SA 4.0

TABLE 1
DEMOGRAPHIC AND CLINICAL CHARACTERISTICS OF THE SOURCE COHORT

Variable	PD (*n* = 20)	Control (*n* = 20)	p-value
Age, years	69.9 ± 10.1	65.6 ± 9.9	0.23
Men, %	60	45	0.52
Education, years	9.3 ± 4.1	12.1 ± 5.2	0.06
MoCA	21.6 ± 3.8	26.2 ± 2.7	<0.001
MDS-UPDRS III	37.4 ± 18.6	—	—
Disease duration, years	8.2 ± 3.8	—	—
Hoehn and Yahr	2.9 (2–4)	—	—

Note: Values correspond to the original 40-participant source cohort.

B. fNIRS Acquisition and Experimental Protocol

1) fNIRS Acquisition

Cortical hemodynamics were acquired using a portable continuous-wave Brite MKII system (Artinis Medical Systems BV, The Netherlands), with 10 dual-wavelength sources centered at 757 and 843 nm and eight detectors. The optode configuration generated 20 long-separation channels distributed across bilateral motor regions and two short-separation measurements. Long source-detector separation was approximately 3 cm and short separation approximately 1.5 cm [4]. The bilateral motor-cortex optode montage used for data acquisition is shown in Fig. 2.

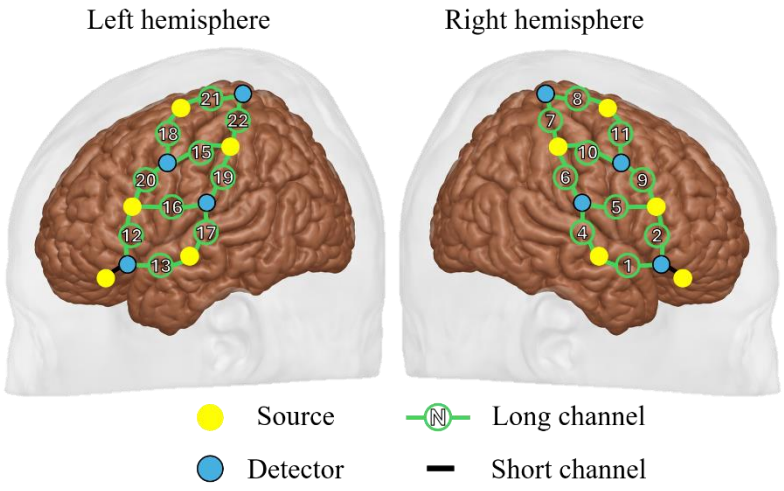

Fig. 2. Bilateral motor-cortex fNIRS optode montage used in the original acquisition. Long-separation channels were used for cortical spectral analysis, whereas short-separation positions 3 and 14 were excluded from participant-level β feature extraction. Source and detector locations are identified according to the legend. Adapted from Guevara et al. [4].

CC BY-NC-SA 4.0

Científica, vol. 30, no. 2, pp. 01-16, July-December 2026,
ISSN 2594-2921, Instituto Politécnico Nacional, MÉXICO
e300211 | DOI: 10.46842/ipn.cien.v30n2a11

2) Finger-tapping Task

Participants consecutively opposed the thumb to the remaining fingers of one hand. Movement was performed in 10-s blocks separated by variable rest periods of approximately 20–24 s. Twenty blocks were completed, 10 for each hand, in randomized order, and the complete task lasted approximately 11 min [4].

3) Walking Task

Participants completed approximately 2 min of over-ground walking along a 6-m path with 180° turns at each end. A member of the research team accompanied each participant for safety [4].

4) Resting-State Acquisition

Participants remained seated for approximately 6 min with eyes closed in a dimly lit room and were instructed to remain relaxed, awake, and as motionless as possible [4].

C. Homer3 Preprocessing

The present study did not reprocess raw optical-intensity data. The input of the Python spectral pipeline consisted of the final continuous hemoglobin-concentration time series obtained from the previously established Homer3 preprocessing workflow. This preprocessing included channel-quality pruning, conversion from raw intensity to optical density, motion-artifact identification and correction, temporal filtering, and conversion to hemoglobin concentration using the modified Beer–Lambert law [4], [9].

The original acquisition also included two short-separation measurements. These measurements were used in the previously reported GLM-based analysis for hemodynamic response function (HRF) estimation [4], but short-separation regression was not applied to the continuous concentration time series analyzed in the present spectral study. Accordingly, the current analysis was performed on the continuous HbO, HbR, and HbT signals rather than on GLM-derived HRF estimates.

The exported matrices contained one time vector and 22 columns for each chromophore (HbO, HbR, and HbT). Positions 3 and 14 corresponded to the short-separation measurements and were excluded from cortical spectral feature extraction, leaving 20 long-separation cortical channels. No additional temporal band-pass filtering was applied during the present Python analysis. The only frequency-selective operation introduced in Python was the anti-alias filtering inherent to polyphase downsampling for recordings acquired above 25 Hz.

D. Sampling-Frequency Quality Control and Resampling

The first column of each exported file contained time information. The original sampling frequency of each recording was estimated from the mean positive temporal increment according to equation (1).

$$F_s = \frac{1}{mean(\Delta t)} \tag{1}$$

Timestamp inspection identified recordings at 25, 50, and 75 Hz. Among the 116 recordings retained after final duration quality control, 99 (85.3%) were acquired at 25 Hz, 12 (10.3%) at 50 Hz, and five (4.3%) at 75 Hz. Recordings

CC BY-NC-SA 4.0

already acquired at 25 Hz were used directly, whereas recordings at 50 or 75 Hz were downsampled to 25 Hz using polyphase resampling. The complete list of recordings acquired above 25 Hz is provided in Supplementary Table S1.

E. Duration Standardization and Participant Selection

Because recording durations varied slightly between participants, fixed task-specific common windows were used so that every retained participant contributed the same observation time within each paradigm. After resampling to 25 Hz, signals were truncated to 265 s for resting state, 590 s for finger tapping, and 118 s for walking.

The original dataset contained 120 participant-task recordings. Of these, 116 satisfied the final common-duration requirement. Four recordings remained too short: finger tapping from Control18 (328.96 s), resting state from Control19 (178.04 s), resting state from Control20 (178.04 s), and resting state from PD20 (175.04 s). Consequently, the final complete-case three-task cohort comprised 36 participants: 17 controls and 19 participants with PD. The participant and recording selection process is summarized in Fig. 3.

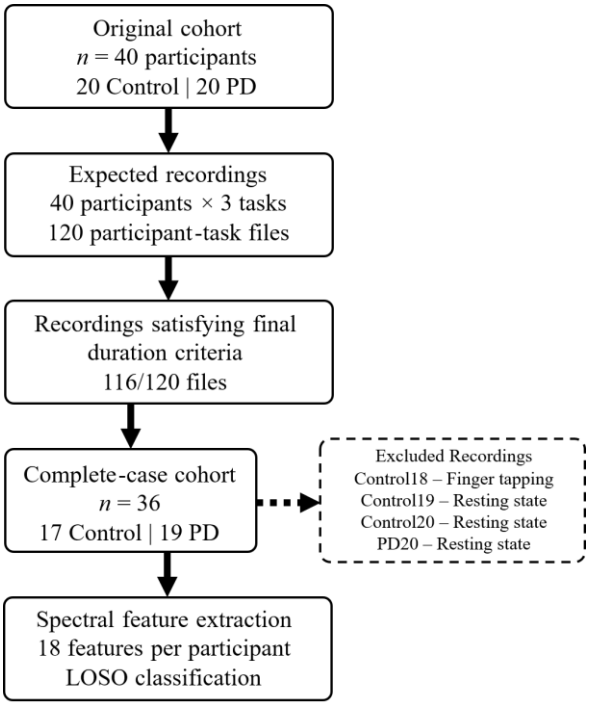

Fig. 3. Participant and recording selection for the final three-task analysis. The original dataset comprised 40 participants (20 controls and 20 participants with Parkinson's disease [PD]) and 120 participant-task recordings. After sampling-frequency harmonization and task-specific duration quality control, 116 recordings were retained. Four participants lacked a complete set of eligible recordings, resulting in a final complete-case cohort of 36 participants (17 controls and 19 PD) for spectral feature extraction and LOSO classification.

CC BY-NC-SA 4.0

Científica, vol. 30, no. 2, pp. 01-16, July-December 2026,
ISSN 2594-2921, Instituto Politécnico Nacional, México
e300211 | DOI: 10.46842/ipn.cien.v30n2a11

F. Power Spectral Density Estimation

Power spectral density was estimated independently for every retained cortical channel and chromophore using Welch's averaged periodogram method [12]. The analysis used $F_s = 25\,Hz$, a Hann window, Nperseg = 2048, Noverlap = 1024, NFFT = 2048, density scaling, and no additional detrending in the Welch call.

$$P(f) \propto f^{-\beta} \tag{2}$$

$$\log_{10}[P(f)] = C - \beta \log_{10}(f) \tag{3}$$

The nominal frequency resolution was given by equation (4). The zero-frequency bin was excluded from logarithmic analysis.

$$\Delta f = \frac{25}{2048} = 0.012207\ Hz \tag{4}$$

G. Dual-Slope Spectral Model

Rather than fitting two unrelated straight lines, a continuous segmented regression was fitted in logarithmic coordinates. Let $x = \log_{10}(f)$, $y = \log_{10}[P(f)]$, and $x_c = \log_{10}(f_c)$. The model was defined by equation (5).

$$y = a + b_1 x + \delta \max(0, x - x_c) \tag{5}$$

The corresponding spectral descriptors were defined as the negative slopes of the two regions:

$$\beta_1 = -b_1 \tag{6}$$

$$\beta_2 = -(b_1 + \delta) \tag{7}$$

Continuity at the crossover avoided an arbitrary vertical discontinuity between the low- and high-frequency regression segments. Model fit was quantified using residual sum of squares, RMSE, segment-specific R^2, total R^2, and a robust normalized RMSE (NRMSE) using the 5th–95th percentile range of log10 power.

H. Spectral Configurations

Four exploratory configurations were evaluated. The 10- and 12.5-Hz values were upper limits of the PSD bins included in the regression and did not represent additional temporal filtering of the signals.

TABLE 2
SPECTRAL CONFIGURATIONS EVALUATED

Configuration	Crossover	Upper frequency
Fixed-10	Task-specific fixed	10 Hz
Fixed-12.5	Task-specific fixed	12.5 Hz
Auto-10	NRMSE optimized	10 Hz
Auto-12.5	NRMSE optimized	12.5 Hz

CC BY-NC-SA 4.0

The fixed crossover frequencies were 0.100 Hz for resting state, 3.162 Hz for finger tapping, and 0.562 Hz for walking. These values were retained as exploratory reference points and were not interpreted as previously established physiological boundaries.

I. Automatic Crossover Selection

Automatic crossover estimation was performed independently for each task but jointly across HbO, HbR, HbT and both diagnostic groups. Diagnostic labels were not used to determine the crossover. Candidate frequencies corresponded to Welch bins and were constrained to avoid trivial splits near the frequency limits. Each candidate required at least eight spectral points below the crossover, 30 above it, a minimum lower-segment span of 0.40 logarithmic decades, and an upper-segment span of at least 0.30 decades.

$$f_c^* = \arg\min_{f_c} \text{median}(\text{NRMSE}) \tag{8}$$

For classification using automatic configurations, the crossover search was repeated inside every LOSO training fold so that the held-out participant could not influence f_c.

J. Participant-Level Feature Extraction

For each participant, task, and chromophore, β_1 and β_2 were calculated for each valid long-separation cortical channel. Participant-level values were obtained as the median across the 20 cortical channels. Each task therefore contributed six features (β_1 and β_2 for HbO, HbR, and HbT), giving 18 features across the three paradigms.

$$3\ tasks \times 3\ chromophores \times 2\ slopes = 18\ features \tag{9}$$

No supervised feature-subset selection was performed before classification.

K. Classification and LOSO Validation

Classification was implemented in Python using scikit-learn [13], with numerical routines from SciPy [14]. The pipeline consisted of StandardScaler, principal component analysis (PCA) retaining 95% of the training-set variance, and L2-regularized logistic regression. PD was treated as the positive class and a fixed probability threshold of 0.50 was used for confusion-matrix predictions.

Generalization within the available cohort was estimated using leave-one-subject-out cross-validation (LOSO). In each of 36 outer folds, 35 participants were used for training and one participant was completely withheld for testing. Feature scaling, PCA, logistic-regression fitting, and—when applicable—automatic crossover estimation were performed using training participants only. Each participant therefore received one fully out-of-sample probability. Across folds, the median number of retained principal components was five.

L. Performance Metrics and Permutation Analysis

Classification performance was summarized using accuracy, balanced accuracy, sensitivity, specificity, precision for PD, F1 score, Matthews correlation coefficient (MCC), and ROC-AUC. ROC-AUC was calculated from the continuous LOSO probabilities and was therefore independent of the fixed 0.50 decision threshold. Chance-level

CC BY-NC-SA 4.0

performance was assessed using 500 random permutations of diagnostic labels. Empirical p-values were calculated according to equation (10).

$$\text{pperm} = \frac{[1 + \#(\text{Mperm} \geq \text{Mobs})]}{(\text{Nperm} + 1)} \quad (10)$$

With 500 permutations, the minimum possible empirical p-value was 1/501 = 0.001996.

III. Results

A. Dataset Retention and Sampling-Frequency Quality Control

Of the 120 expected participant-task recordings, 116 satisfied the final common-duration criteria. The final complete-case cohort included 36 participants: 17 controls and 19 participants with PD. Timestamp-based verification identified 99 recordings at 25 Hz, 12 at 50 Hz, and five at 75 Hz. All recordings entered subsequent spectral analysis at the common sampling frequency of 25 Hz.

B. Spectral Crossover Estimation

For the complete cohort, Auto-10 selected crossover frequencies of 0.4639 Hz for resting state, 2.9053 Hz for finger tapping, and 0.3296 Hz for walking. Auto-12.5 selected 6.2622 Hz, 2.6733 Hz, and 0.3662 Hz, respectively.

Within nested LOSO, Auto-10 crossover estimates remained stable: 0.4517 [0.4150–0.4517] Hz for resting state, 2.9053 [2.9053–2.9907] Hz for finger tapping, and 0.3296 [0.3296–0.3418] Hz for walking.

TABLE 3
FIXED AND AUTOMATIC CROSSOVER FREQUENCIES

Task	Fixed	Auto-10	Auto-12.5
Resting state	0.100	0.464	6.262
Finger tapping	3.162	2.905	2.673
Walking	0.562	0.330	0.366

C. Spectral Model Fit

Auto-10 provided the lowest global median normalized error (NRMSE = 0.0346) and the strongest overall segmented fit, with median $R_1^2 = 0.8754$, $R_2^2 = 0.9845$, and total $R^2 = 0.9888$. Fixed-10 ranked second by NRMSE, followed by Auto-12.5 and Fixed-12.5.

TABLE 4
GLOBAL GOODNESS OF FIT OF FOUR SPECTRAL CONFIGURATIONS

Configuration	NRMSE	R_1^2	R_2^2	Total R^2
Auto-10	0.0346	0.8754	0.9845	0.9888
Fixed-10	0.0393	0.5614	0.9835	0.9867
Auto-12.5	0.0497	0.8576	0.9470	0.9787
Fixed-12.5	0.0540	0.4774	0.9722	0.9751

CC BY-NC-SA 4.0

Task-level analysis similarly favored Auto-10 for resting state (NRMSE = 0.0302; total R^2 = 0.9931) and walking (NRMSE = 0.0296). For finger tapping, Auto-10 and Fixed-10 yielded closely similar NRMSE values of 0.0448 and 0.0457, respectively. Representative log-log PSD profiles and continuous dual-slope fits for the three experimental paradigms are shown in Fig. 4.

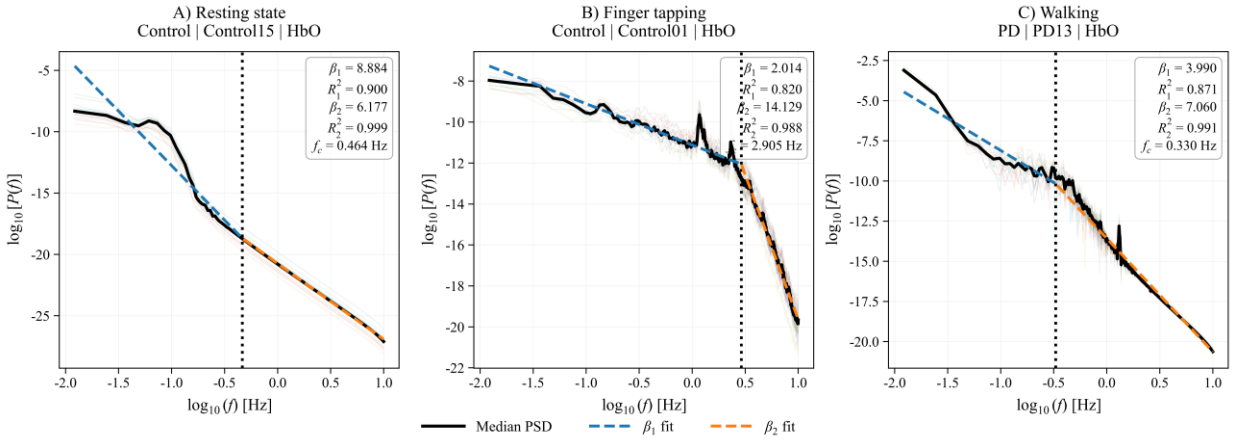

Fig. 4. Representative log-log power spectral density (PSD) profiles and continuous dual-slope fits for the three experimental paradigms. Thin curves represent individual long-separation cortical channels and the emphasized curve represents the participant-level median PSD. The vertical line indicates the estimated crossover frequency f_c, separating the lower-frequency β1 region from the higher-frequency β2 region. Dashed lines indicate the corresponding segmented linear fits in $\log_{10}[P(f)]$ versus $\log_{10}(f)$ space. Representative examples are shown for (A) resting state, (B) finger tapping, and (C) walking.

D. Classification Performance

All four spectral configurations produced participant-level LOSO classification performance above their corresponding permutation distributions. Fixed-12.5 achieved the highest threshold-dependent performance, whereas Auto-10 achieved the highest ROC-AUC.

TABLE 5
LOSO CLASSIFICATION PERFORMANCE

Model	Acc	BA	Sens	Spec	Prec	F1	MCC	AUC	pBA	pAUC
Fixed-10	0.7778	0.7802	0.7368	0.8235	0.8235	0.7778	0.5604	0.8173	0.0020	0.0020
Fixed-12.5	0.8611	0.8622	0.8421	0.8824	0.8889	0.8649	0.7233	0.8204	0.0020	0.0020
Auto-10	0.8333	0.8359	0.7895	0.8824	0.8824	0.8333	0.6718	0.8266	0.0020	0.0020
Auto-12.5	0.8056	0.8065	0.7895	0.8235	0.8333	0.8108	0.6121	0.8111	0.0020	0.0040

Fixed-12.5 correctly classified 15 of 17 controls and 16 of 19 participants with PD, yielding 86.1% accuracy, 86.2% balanced accuracy, 84.2% sensitivity, 88.2% specificity, MCC = 0.723, and ROC-AUC = 0.820. Auto-10 correctly classified 15 of 17 controls and 15 of 19 participants with PD, yielding 83.3% accuracy, 83.6% balanced accuracy, 78.9% sensitivity, 88.2% specificity, MCC = 0.672, and the highest ROC-AUC, 0.827. The corresponding confusion matrices and LOSO ROC curves for the four spectral configurations are shown in Fig. 5.

CC BY-NC-SA 4.0

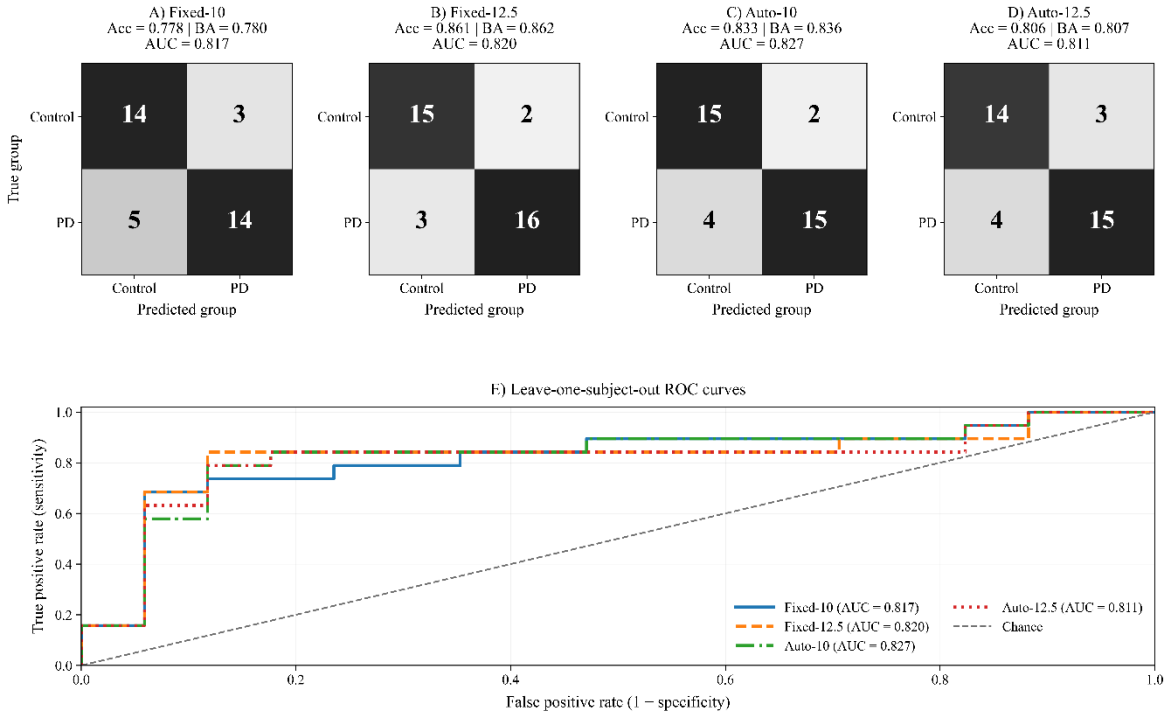

Fig. 5. Participant-level classification performance of the four dual-slope spectral configurations under leave-one-subject-out (LOSO) validation. (A–D) Confusion matrices for Fixed-10, Fixed-12.5, Auto-10, and Auto-12.5, respectively; rows indicate the true diagnostic group and columns indicate the predicted group. (E) Receiver-operating characteristic (ROC) curves obtained from the continuous LOSO probability estimates for the four configurations.

E. Permutation Analysis

For Fixed-10, Fixed-12.5, and Auto-10, the observed balanced accuracy and ROC-AUC reached the minimum p-value permitted by 500 permutations (pperm = 0.001996). For Auto-12.5, balanced accuracy yielded pperm = 0.001996 and ROC-AUC yielded pperm = 0.003992. These values should be interpreted at the resolution provided by the permutation count.

IV. Discussion

A. Main Findings

Three main findings emerged from this exploratory analysis. First, a compact set of 18 task-dependent β_1 and β_2 features contained sufficient multivariate information to separate PD and control participants under participant-wise LOSO validation. Second, classification was comparatively robust across four alternative spectral parameterizations, with ROC-AUC values ranging from 0.811 to 0.827. Third, the configuration that best described the spectral morphology was not identical to the configuration producing the highest 0.50-threshold accuracy: Auto-10 provided the best spectral fit and highest ROC-AUC, whereas Fixed-12.5 produced the highest accuracy and balanced accuracy.

CC BY-NC-SA 4.0

Científica, vol. 30, no. 2, pp. 01-16, July-December 2026,
ISSN 2594-2921, Instituto Politécnico Nacional, México
e300211 | DOI: 10.46842/ipn.cien.v30n2a11

B. Task-Dependent Spectral Information

The inclusion of resting state, finger tapping, and walking allowed each participant to be characterized under three distinct physiological contexts. This is consistent with prior work in the same cohort showing delayed task-evoked motor responses during finger tapping and altered resting-state connectivity, while conventional walking activation did not show an equally clear between-group difference [4], [5]. The present results suggest that a task that is not individually significant under a conventional univariate analysis may still provide complementary multivariate information when combined with other paradigms.

Accordingly, the classifier should not be interpreted as identifying a single "Parkinson frequency." Instead, it uses the joint arrangement of low- and high-frequency spectral slopes across tasks and chromophores. Useful classification therefore does not require each individual β feature to be significantly different between groups.

C. Fixed Versus Automatic Crossover Selection

The automatic crossover analysis addressed whether the two-slope representation could be determined using an objective spectral-fit criterion rather than fixed visual thresholds. Auto-10 produced the lowest NRMSE and highest total R^2, while its training-only crossover estimates remained narrow across LOSO folds. This stability suggests that the selected crossover frequencies were not dictated by one or two influential participants.

Nevertheless, Fixed-12.5 produced the highest threshold-dependent accuracy. This is not contradictory: accuracy depends on a specific probability threshold, whereas ROC-AUC summarizes rank discrimination over all possible thresholds. The most transparent interpretation is therefore that Auto-10 provided the best spectral-model representation and highest rank-based discrimination, whereas Fixed-12.5 yielded the largest number of correct classifications at the prespecified 0.50 threshold. Reporting both results avoids post hoc selection of a single "winning" configuration.

D. Interpretation of the Post-Homer3 Spectrum

The present analysis began from the final continuous Homer3 concentration signals rather than raw optical intensity. The objective was therefore classification from a reproducible processed signal, not recovery of an unfiltered physiological scaling law. β_1 and β_2 quantify the spectral morphology remaining after the established fNIRS preprocessing workflow.

This distinction improves reproducibility of the classification pipeline but limits direct mechanistic interpretation. The observed PSD can reflect cerebral hemodynamics together with residual systemic physiology, motion-correction operations, short-channel handling, the transfer characteristics of the Homer3 filtering stage, and—where required—resampling. Accordingly, the current β values are best regarded as empirical post-processing spectral descriptors. Demonstrating two intrinsic physiological power-law regimes would require a separate analysis explicitly designed for spectral-scaling inference.

E. Interpretation of the 10- and 12.5 Hz Upper Bounds

After harmonization to 25 Hz, the Nyquist frequency was 12.5 Hz. The alternative 10-Hz limit was evaluated as a more conservative regression domain that excludes the extreme Nyquist boundary. Neither value represented an additional temporal filter: the time series was unchanged, and only the PSD bins included in the segmented regression differed.

CC BY-NC-SA 4.0

Auto-10 yielded a substantially lower global NRMSE than Auto-12.5 (0.0346 versus 0.0497), supporting the conclusion that the two-slope model described the post-Homer3 spectra more consistently over the 10-Hz range. However, because the source signals had already undergone Homer3 filtering, 10 Hz should not be interpreted as a physiological upper limit of cortical hemodynamics.

F. Comparison with Previous fNIRS Classification Work

Previous work has demonstrated that fNIRS can contain substantial discriminative information for PD. Guevara et al. extracted 792 temporal and spectral variables and used feature-ranking and genetic feature selection with logistic regression, reporting very high internal classification performance [6]. The present approach intentionally takes a different direction: it uses only 18 participant-level descriptors and no supervised feature-subset search, while retaining participant-wise out-of-sample validation. Therefore, the present results should not be interpreted as superior to earlier work, but rather as evidence that a much more compact spectral representation retains useful disease-associated information.

Related fNIRS studies of scale invariance and fractal behavior also support the idea that temporal organization can provide information complementary to conventional activation measures [7], [8].

G. Methodological Strengths

Several design choices increase the reproducibility of the present exploratory analysis:

- the final Homer3 output was explicitly defined as the starting point of the Python pipeline;
- sampling frequency was audited from the actual timestamps of every recording rather than assumed from the nominal protocol;
- recordings at 50 and 75 Hz were harmonized to a common 25-Hz analysis frequency;
- all retained participants contributed the same duration within each task;
- short-separation positions 3 and 14 were excluded from cortical feature extraction;
- feature standardization and PCA were fitted using training participants only;
- automatic crossover selection was nested within LOSO and did not use diagnostic labels; and
- all four explored spectral configurations were reported together with permutation testing rather than retaining only the numerically best classifier.

H. Limitations

First, the final analysis contained only 36 participants. LOSO ensures that each reported prediction is generated by a model that did not train on that participant, but it remains an internal validation strategy and cannot replace independent external testing.

Second, the present work is a secondary analysis of a cohort previously examined using task-response, connectivity, machine-learning, and nonlinear approaches. The results therefore represent further characterization of a known dataset rather than independent replication.

Third, the analytical framework (including the two-slope representation, the fixed crossover reference values, and the comparison between 10- and 12.5-Hz upper limits) was developed exploratorily using the current cohort.

CC BY-NC-SA 4.0

Fourth, the analyzed time series were final post-Homer3 signals. β_1 and β_2 may therefore reflect both biological signal structure and characteristics introduced by previous preprocessing, limiting their direct interpretation as intrinsic physiological exponents.

Fifth, the original sampling frequency was not uniform across recording sessions. Polyphase resampling standardized all data to 25 Hz, but residual session-specific acquisition effects cannot be completely excluded.

Sixth, the three tasks had substantially different usable durations. With Nperseg = 2048 at 25 Hz, one Welch segment spans 81.92 s; consequently, the 118-s walking recording supports fewer averaged segments than resting state or finger tapping and therefore has intrinsically greater PSD variance.

Seventh, HbT is mathematically related to HbO and HbR, so the 18 raw features are not independent. PCA reduces part of this redundancy, with a median of five retained components per fold.

Eighth, cognition differed between PD and control participants in the original cohort, and the final classifier may therefore capture a mixture of disease-associated motor, cognitive, vascular, and hemodynamic differences rather than a PD-specific motor signature alone.

Finally, 500 permutations limit the resolution of empirical p-values to approximately 0.002. A future locked analysis may increase the number of permutations without modifying any model parameters.

V. Conclusion

Task-specific β_1 and β_2 dual-slope spectral features derived from post-Homer3 motor-cortex fNIRS recordings provided a compact representation capable of internally discriminating participants with Parkinson's disease from healthy controls. Across four spectral parameterizations, LOSO accuracy ranged from 77.8% to 86.1% and ROC-AUC from 0.811 to 0.827. Fixed-12.5 produced the highest threshold-dependent accuracy and balanced accuracy, whereas Auto-10 provided the best spectral fit and highest ROC-AUC. All configurations exceeded their corresponding permutation null distributions.

These findings support further investigation of task-dependent fNIRS spectral morphology as a low-dimensional representation of PD-associated motor-network alterations. Because β_1 and β_2 were derived from final Homer3-processed signals, they should presently be interpreted as empirical spectral descriptors rather than direct estimates of intrinsic physiological scaling. External validation using a locked analytical pipeline is required before considering diagnostic applications.

CRediT (*Contributor Roles Taxonomy*)

Author Contributions: Conceptualization: JF**CM**, E**G**; Methodology: JF**CM**, D**AM**, E**G**; Software: JF**CM**; Investigation: D**AM**, G**FM**, CL**TP**, G**VM**, A**VH**, E**G**; Formal analysis: JF**CM**, D**AM**; Writing—original draft preparation: JF**CM**; Writing—review and editing: JF**CM**, D**AM**, G**FM**, CL**TP**, G**VM**, A**VH**, E**G**; Supervision: AVH, E**G**; Project administration: E**G**.

Funding: The authors are thankful to SECIHTI for J.F.C.-M.'s scholarship.

Data Availability Statement: The raw fNIRS data supporting this study are publicly available in the Zenodo repository at https://doi.org/10.5281/zenodo.7966829. The processed data and derived analysis outputs used in the present study may be available from the corresponding author upon reasonable request.

Aknowledgement: The authors acknowledge the participants and clinical/research personnel involved in the original fNIRS acquisition and thank Cinvestav's bibliographic services.

Conflicts of Interest: The authors declare no conflicts of interest.

CC BY-NC-SA 4.0

REFERENCES

[1] J. Jankovic, "Parkinson's disease: clinical features and diagnosis," *Journal of Neurology, Neurosurgery & Psychiatry*, vol. 79, no. 4, pp. 368–376, 2008, doi: https://doi.org/10.1136/jnnp.2007.131045

[2] W. Poewe, K. Seppi, C. M. Tanner, et al., "Parkinson disease," *Nature Reviews Disease Primers*, vol. 3, Art. no. 17013, 2017, doi: https://doi.org/10.1038/nrdp.2017.13

[3] F. Scholkmann, S. Kleiser, A. J. Metz, et al., "A review on continuous wave functional near-infrared spectroscopy and imaging instrumentation and methodology," *NeuroImage*, vol. 85, pt. 1, pp. 6–27, 2014, doi: https://doi.org/10.1016/j.neuroimage.2013.05.004

[4] E. Guevara, F. J. Rivas-Ruvalcaba, E. S. Kolosovas-Machuca, et al., "Parkinson's disease patients show delayed hemodynamic changes in primary motor cortex in fine motor tasks and decreased resting-state interhemispheric functional connectivity: a functional near-infrared spectroscopy study," *Neurophotonics*, vol. 11, no. 2, Art. no. 025004, 2024, doi: https://doi.org/10.1117/1.NPh.11.2.025004

[5] E. Guevara, E. S. Kolosovas-Machuca, I. Rodríguez-Leyva, "Exploring motor cortex functional connectivity in Parkinson's disease using fNIRS," *Brain Organoid and Systems Neuroscience Journal*, vol. 2, pp. 23–30, 2024, doi: https://doi.org/10.1016/j.bosn.2024.04.001

[6] E. Guevara, G. Solana-Lavalle, R. Rosas-Romero, "Integrating fNIRS and machine learning: shedding light on Parkinson's disease detection," *EXCLI Journal*, vol. 23, pp. 763–771, 2024, doi: https://doi.org/10.17179/excli2024-7151

[7] L. Zhu, S. Haghani, L. Najafizadeh, "On fractality of functional near-infrared spectroscopy signals: analysis and applications," *Neurophotonics*, vol. 7, no. 2, Art. no. 025001, 2020, doi: https://doi.org/10.1117/1.NPh.7.2.025001

[8] C. Zhuang, K. L. Meidenbauer, O. Kardan, et al., "Scale invariance in fNIRS as a measurement of cognitive load," Cortex, vol. 154, pp. 62–76, 2022, doi: https://doi.org/10.1016/j.cortex.2022.05.009

[9] T. J. Huppert, S. G. Diamond, M. A. Franceschini, D. A. Boas, "HomER: a review of time-series analysis methods for near-infrared spectroscopy of the brain," *Applied Optics*, vol. 48, no. 10, pp. D280–D298, 2009, doi: https://doi.org/10.1364/AO.48.00D280

[10] S. Brigadoi, R. J. Cooper, "How short is short? Optimum source–detector distance for short-separation channels in functional near-infrared spectroscopy," *Neurophotonics*, vol. 2, no. 2, Art. no. 025005, 2015, doi: https://doi.org/10.1117/1.NPh.2.2.025005

[11] I. Tachtsidis and F. Scholkmann, "False positives and false negatives in functional near-infrared spectroscopy: issues, challenges, and the way forward," *Neurophotonics*, vol. 3, no. 3, Art. no. 031405, 2016.

[12] P. D. Welch, "The use of fast Fourier transform for the estimation of power spectra: a method based on time averaging over short, modified periodograms," *IEEE Transactions on Audio and Electroacoustics*, vol. 15, no. 2, pp. 70–73, Jun. 1967, doi: https://doi.org/10.1109/TAU.1967.1161901

[13] F. Pedregosa, G. Varoquaux, A. Gramfort, et al., "Scikit-learn: Machine Learning in Python," Journal of Machine Learning Research, vol. 12, pp. 2825–2830, 2011.

[14] P. Virtanen, R. Gommers, T. E. Oliphant, et al., "SciPy 1.0: fundamental algorithms for scientific computing in Python," *Nature Methods*, vol. 17, pp. 261–272, 2020, doi: https://doi.org/10.1038/s41592-019-0686-2 .

CC BY-NC-SA 4.0

Científica, vol. 30, no. 2, pp. 01-16, July-December 2026,
ISSN 2594-2921, Instituto Politécnico Nacional, MÉXICO
e300211 | DOI: 10.46842/ipn.cien.v30n2a11